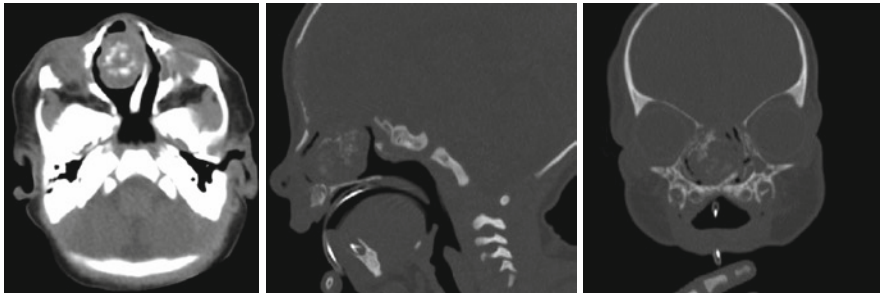
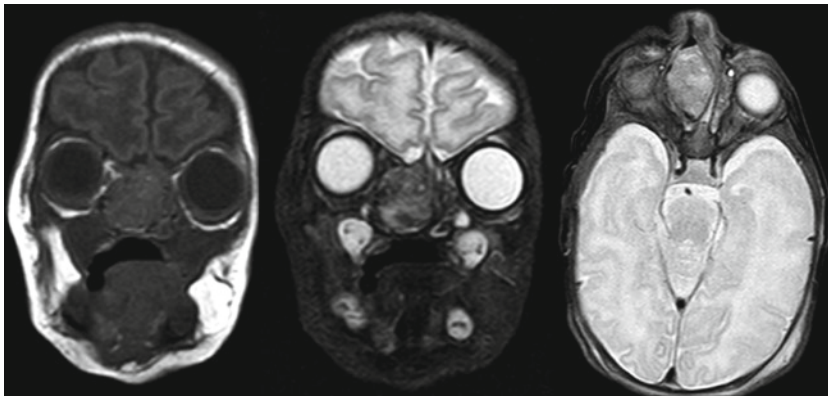
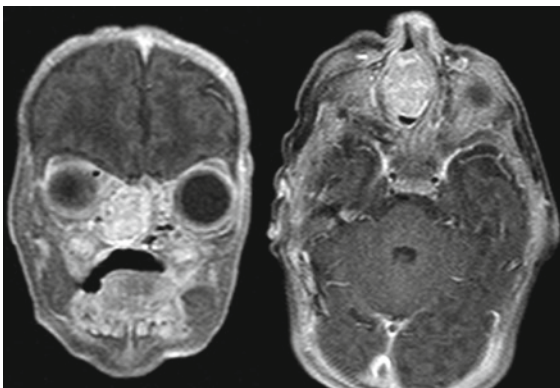
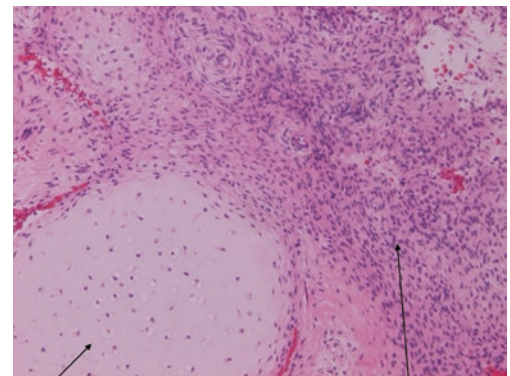


## Contents

<b>Case 2.1</b>	<b>Nasal Chondromesenchymal Hamartoma</b> . . . . .	26
	L. Santiago Medina and Sara M. Koenig	
<b>Case 2.2</b>	<b>Pleomorphic Xanthoastrocytoma</b> . . . . .	28
	Francisco Menor Serrano and María Jesús Esteban Ricós	
<b>Case 2.3</b>	<b>Desmoplastic Infantile Ganglioglioma</b> . . . . .	30
	María I. Martínez León	
<b>Case 2.4</b>	<b>Dysembryoplastic Neuroepithelial Tumor of the Septum Pellucidum (DNET SP)</b> . . . . .	32
	María I. Martínez León and Bernardo Weil Lara	
<b>Case 2.5</b>	<b>CNS Langerhans Cell Histiocytosis</b> . . . . .	34
	Diego Alcaide Martín and María I. Martínez León	
<b>Case 2.6</b>	<b>Hemangioma of Infancy</b> . . . . .	36
	Cristina Bravo Bravo and Pascual García-Herrera Taillefer	
<b>Case 2.7</b>	<b>Vascular Lesion of the Face</b> . . . . .	38
	Sara M. Koenig and Juan E. Gutiérrez	
<b>Case 2.8</b>	<b>Retinoblastoma</b> . . . . .	40
	Juan E. Gutiérrez and Sara M. Koenig	
<b>Case 2.9</b>	<b>Tuberous Sclerosis</b> . . . . .	42
	Ana Alonso Murciano and María I. Martínez León	
<b>Case 2.10</b>	<b>Neurofibromatosis Type 1</b> . . . . .	44
	Inés Solís Muñiz	

**Case 2.1****Nasal Chondromesenchymal Hamartoma**

L. Santiago Medina and Sara M. Koenig

**Fig. 2.1****Fig. 2.2****Fig. 2.3****Chondroid areas****Mesenchymal areas****Fig. 2.4**

A 3-day-old neonate develops cyanosis during feeding. MRI reveals a large mass in the sinonasal region, calcifications, and erosion of adjacent bony structures.

Nasal chondromesenchymal hamartoma is very rare and benign ossifying fibromyxoid tumor, and it most commonly presents during infancy as a congenital condition, although it may present later in childhood. It must be distinguished from other masses such as a dermoid teratoma, nasal glioma, and esthesioneuroblastoma as well as other chondroid, angiomatous, or lipomatous hamartomas. A hamartoma is a tumor-like formation that originates from excessive growth of tissues native to the site of origin, unlike a teratoma known to be caused by excessive growth of pluripotential cells foreign to the site of origin. Additional presenting symptoms of nasal chondromesenchymal hamartomas include deficits or impairment of eye movement (unilaterally), asymmetry of the face, asymmetric maxillary swelling, difficulty or inability to breathe nasally, and protruding nasal polyps.

Histologically, a chondromesenchymal hamartoma consists of proliferative lobules of cartilage with contiguous spindle cells and myxoid areas of mesenchymal tissue, as well as extensive RER and Golgi complexes and microfilamentous bundles within the cells.

Treatment typically involves complete resection of the aberrant tissue. In this case, a septoplasty and right middle turbinectomy were also performed. Recurrence is common after an incomplete resection, but the tumor typically remains as a microscopic residual tumor. No adjuvant therapy is necessary.

Axial, sagittal, and coronal CT images show irregular broad-based mass located in the anterior and medial nasal fossa on the right with multiple calcifications, mass effect to the surrounding structures, and deviating the nasal septum to the left (Fig. 2.1a–c). Coronal T1-weighted and coronal and axial Fat Sat (FS) T2-weighted MR images demonstrate the mass being iso- to hypointense in a T1-weighted MR image and slightly hyperintense in a T2-weighted image with well-defined margins and calcifications better defined on CT. No apparent extension to the brain or orbits (Fig. 2.2a–c). T1-weighted FS coronal and axial images with contrast show homogeneous and intense contrast enhancement with adequate border delineation of the lesion without intracranial or intraconal extension (Fig. 2.3a, b). Biopsy specimen pathology slide confirmed the diagnosis (Fig. 2.4).

Figure 2.1

Figure 2.2

Figure 2.3

Figure 2.4

**Acknowledgment** Acknowledgment to Dr. Raj Palani for their help on the preparation of this case.

## Comments

## Image Findings

## Case 2.2

### Pleomorphic Xanthoastrocytoma

Francisco Menor Serrano and María Jesús Esteban Ricós

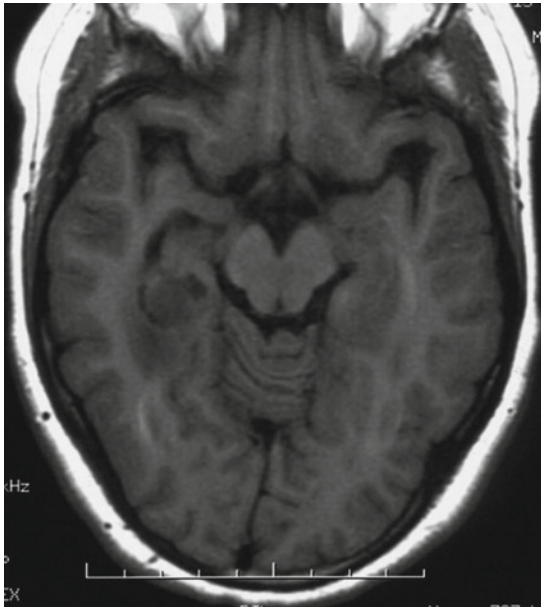


Fig. 2.5

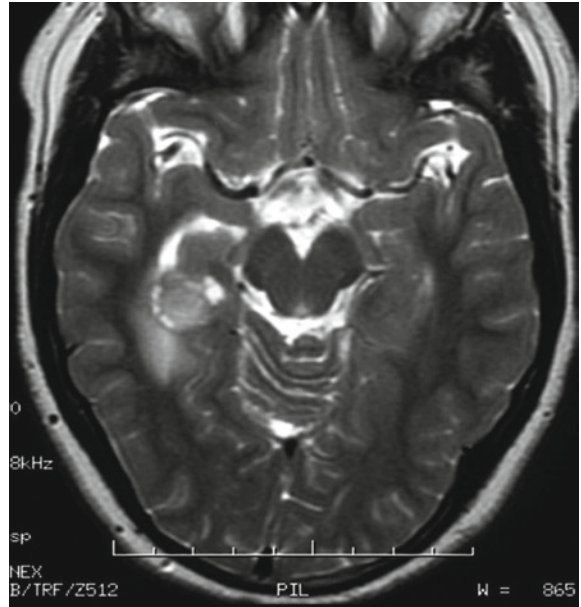


Fig. 2.6

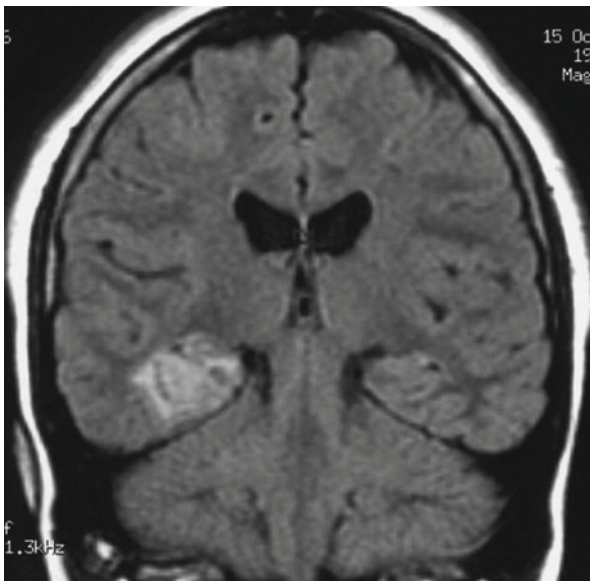


Fig. 2.7

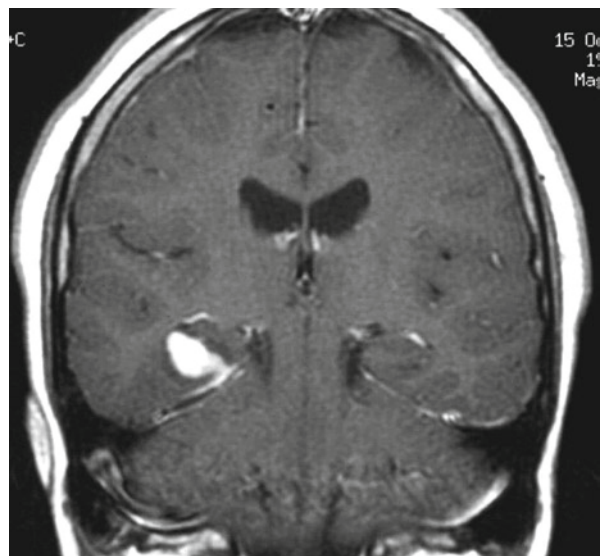


Fig. 2.8

An 11-year-old boy presents with sudden-onset focal left arm seizure.

Pleomorphic xanthoastrocytoma (PXA) is a rare, superficially located tumor arising from subpial astrocytes and often showing extensive involvement of the leptomeninges. Kepes et al. coined the term PXA to describe this tumor in 1979 and it was added to the WHO classification in 1993 as a grade II tumor. PXA is associated with a higher frequency of recurrence, anaplastic transformation, and death in comparison with other low-grade gliomas. Extent of primary resection is a significant factor in the prediction of recurrence-free survival. Response to chemo- and radiotherapy is uncertain. Isolated cases with widespread neuro-axis dissemination at diagnosis and some observations of PXA forming part of both ganglioglioma and dysembryoplastic neuroepithelial tumor have been reported. PXA is rarely diagnosed in infants, being discovered most commonly in adolescents and young adults. The most common single location of PXA is the temporal lobe (50%) and affected patients commonly present with seizures. PXA is uncommon in the basal ganglia, cerebellum, and spinal cord.

The classical, although nonspecific, appearance of PXA is a well-circumscribed superficial temporal solid-cystic mass. Solid components usually exhibit iso-attenuation in relation to gray matter on CT, iso or slightly hypo-intensity on T1-weighted images, iso or mildly hyper-intensity on T2-weighted images, and hyperintensity on FLAIR images and significant contrast enhancement. Calcification is variable and hemorrhage is rare. Large or small cysts are present in about 50% of cases. Surrounding vasogenic edema is usually minimal or absent. Leptomeningeal contrast enhancement is a distinctive finding, seen in more than two thirds of MRI studies.

Axial SE T1-weighted (Fig. 2.5) and T2-weighted MR images (Fig. 2.6) show a right, predominantly solid temporal lobe mass with small peripheral cysts surrounded by edema. The solid component is slightly hypointense on T1-weighted MRI and mildly hyperintense on T2-weighted MR images compared to gray matter. On coronal FLAIR MR images, the tumor exhibits greater hyperintensity, being difficult to make it out from surrounding vasogenic edema; note the small peripheral cysts being hyperintense in comparison to the ventricles (Fig. 2.7). Coronal post-contrast image demonstrates intense contrast enhancement of both the solid tumoral component and adjacent leptomeninges (Fig. 2.8. Reprinted with permission of Editorial Médica Panamericana; Menor F. Imagen en Oncología 2009).

Figure 2.5

Figure 2.6

Figure 2.7

Figure 2.8

## Comments

## Imaging Findings



### Case 2.3

## Desmoplastic Infantile Ganglioglioma

María I. Martínez León



Fig. 2.9

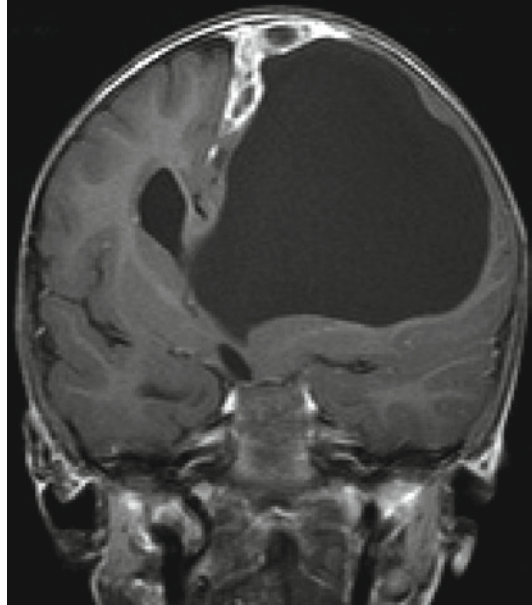


Fig. 2.10

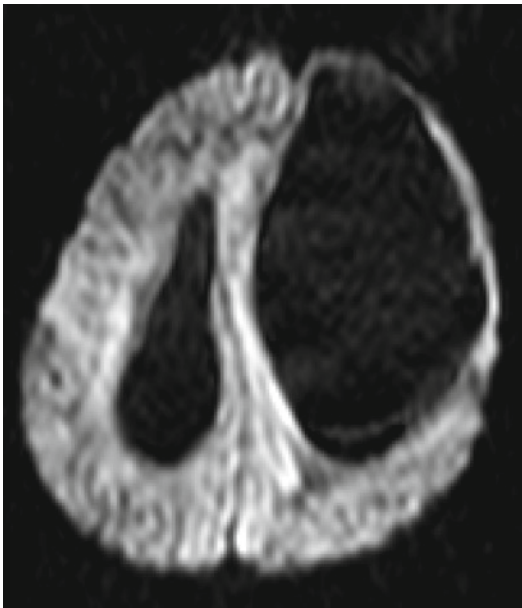


Fig. 2.11



Fig. 2.12

A 27-month-old boy presents with a single epileptic seizure episode. On physical examination, the infant had a protruding forehead on the left side.

Desmoplastic Infantile Ganglioglioma (DIG) is a rare, benign intracranial neoplasm of early childhood with involvement of the superficial cerebral cortex and leptomeninges. They are usually large, predominantly cystic tumors located in the frontal or parietal lobes. DIGs are classified as a benign WHO grade I tumor of infancy and consist of an uncommon variety of ganglioglioma that occur exclusively in infants. Seizures are the most common clinical symptom. Also, a rapidly enlarging head size may be seen.

With CT, a heterogeneous mass containing both a solid and cystic component is identified. With MR T1-weighted imaging, the solid portion of the tumor is isointense relative to normal brain parenchyma and demonstrates significant contrast enhancement. The cystic component has a low signal intensity on T1-weighted MR images and a high signal intensity on T2-weighted MR images. MR spectroscopy shows a lower NAA/creatine ratio, a higher choline/creatine ratio, and no significant change in myoinositol/creatinine ratio. This study may aid in narrowing down the diagnosis.

The differential diagnoses, based on the neuroimaging findings, are primarily, cystic supratentorial astrocytomas, and secondly, high-grade astrocytomas, PNETs, and ependymomas. If the leptomeningeal component of the tumor is large, meningioma and meningeal sarcoma are other possible considerations.

Total resection of the tumor may be curative, eliminating the need for chemotherapy or radiation.

Axial T2-weighted MR image revealed a large supratentorial, predominantly cystic tumor in the left cerebral hemisphere, displacing midline structures to the right. Additionally, the left lateral ventricle is effaced and displaced (Fig. 2.9). Coronal T1-weighted MR image with contrast shows a large cystic component with strong enhancement of a solid mural portion. Contrast enhancement is not seen in the walls of the cyst and the solid component is widely attached to the dura (arrow) (Fig. 2.10). MR diffusion-weighted imaging shows no restriction of the solid or cystic components (Fig. 2.11). MR venography was done before surgical intervention to highlight the absence of longitudinal superior sinus involvement (Fig. 2.12). Tumor was completely resected with surgery and the histological diagnosis was DIG. No recurrence was documented on follow-up examinations.

Figure 2.9

Figure 2.10

Figure 2.11

Figure 2.12

## Comments

## Imaging Findings

**Case 2.4****Dysembryoplastic Neuroepithelial Tumor of the Septum Pellucidum (DNET SP)**

■  
María I. Martínez León and Bernardo Weil Lara

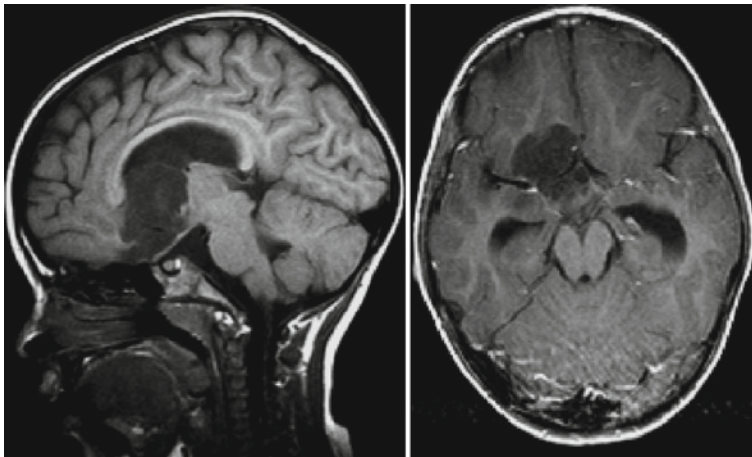


**Fig. 2.13**



**Fig. 2.14**

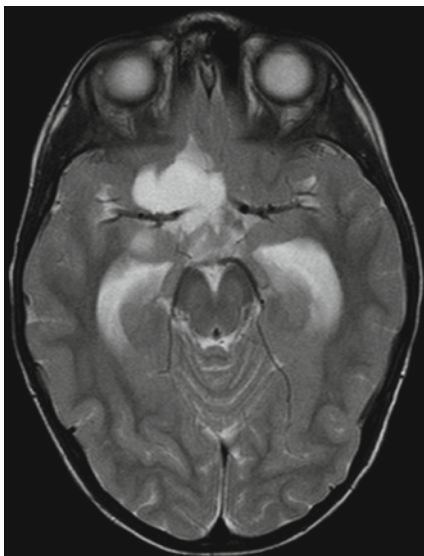


**Fig. 2.15**

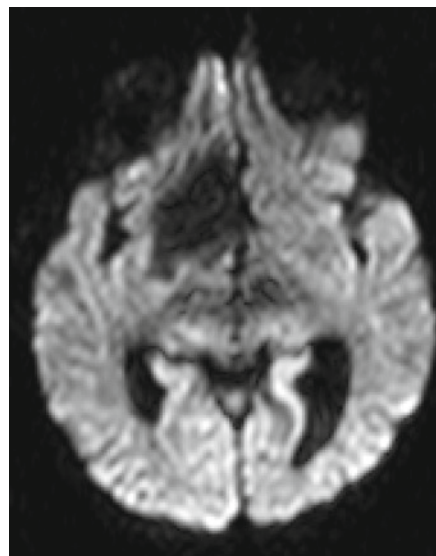


**Fig. 2.16**



A 3-year-old girl presents with headache.

DNET SP are low-grade neoplasms arising at the midline, in the region of the septum pellucidum, with many of the histological features of the DNET. Imaging shows tumors extending into the lateral ventricles from the septal region and obstructing the foramen of Monro causing varying degrees of hydrocephalus. The lesions are lobular, well-delineated, internally septated, hypointense to gray matter on T1-weighted MR images, and hyperintense on T2-weighted MR images. There is usually no mass effect nor is there edema. Diffusion is not restricted and ADC map is high (may be attributable to the presence of large extracellular spaces and their low cellularity). DNET SP is usually non-enhancing or shows only minimal peripheral contrast uptake.

This neoplasm presents with the histological features of DNET, including the “specific glioneuronal element,” a histopathological hallmark characterized by axon bundles that form columns lined by small oligodendroglial-like cells.

First line of treatment is surgical resection and adjuvant chemotherapy or radiotherapy is not commonly needed.

On the basis of both neuroimaging and histopathology, DNET-like lesions should be considered as a differential diagnosis of midline, intraventricular tumors in children and young adults. Differentiating these tumors from more aggressive neoplasms is essential because of the benign evolution DNET SP.

There is a mass located in the anterior recesses of the third ventricle. Sagittal T1-weighted MR images without contrast and axial, T1-weighted MR images with contrast show its location with caudal extension to the suprachiasmatic recess and cranial extension to the intraventricular midline. Signal intensity is slightly increased in relation to CSF in T1-weighted MR images and there is no enhancement with contrast (Fig. 2.13 a, b). A slightly high signal similar to CSF can be appreciated on FLAIR sequences (Fig. 2.14), along with secondary ventricular dilatation due to obstruction of the foramen of Monro. T2-weighted MR image shows a signal similar to that of the CSF. Note that the vessels are encased by the tumor without alteration (Fig. 2.15). No restriction on DWI is identified (Fig. 2.16). According to the location, signal intensity, and behavioral pattern, the findings are indicative of DNET SP. There is histological confirmation of the radiological diagnosis.

Figure 2.13

Figure 2.14

Figure 2.15

Figure 2.16

## Comments

## Imaging Findings

## Case 2.5

### CNS Langerhans Cell Histiocytosis

Diego Alcaide Martín and María I. Martínez León



Fig. 2.17

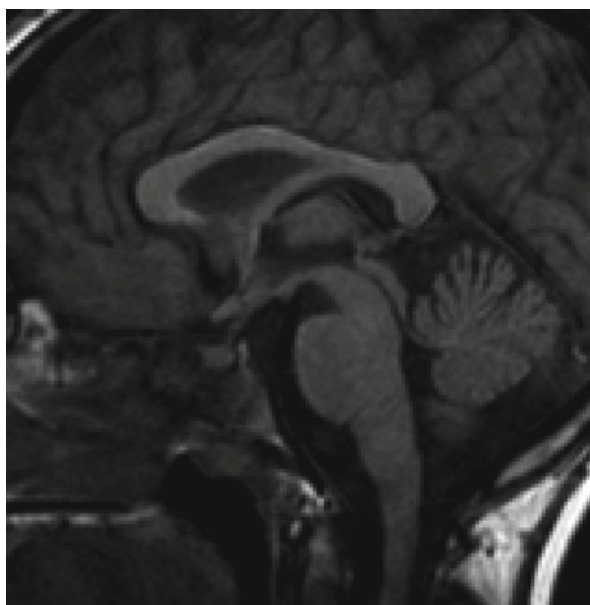


Fig. 2.18

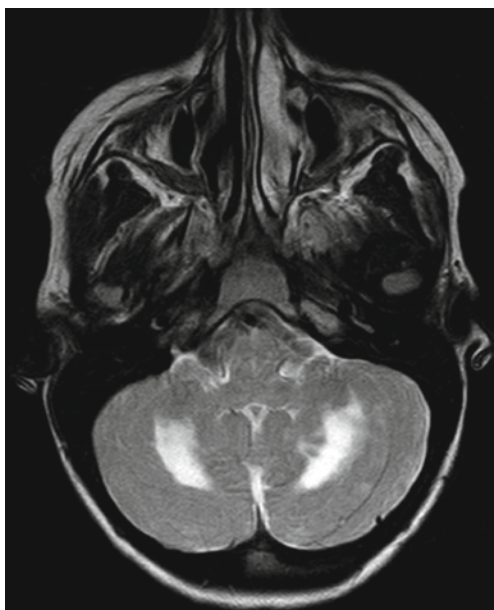


Fig. 2.19

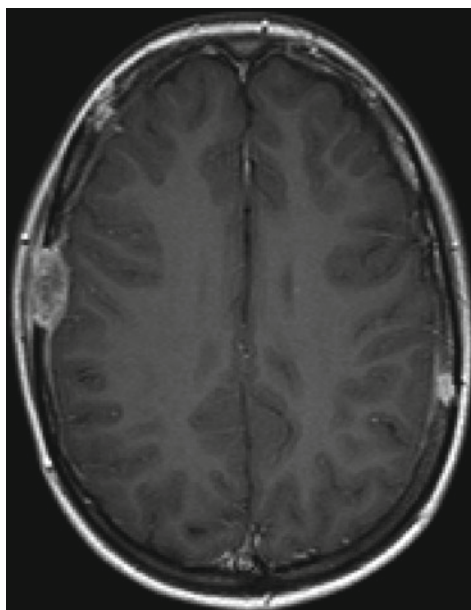


Fig. 2.20

A 15-year-old patient was sent to the endocrinology department for assessment of diabetes insipidus.

Langerhans cell histiocytosis (LCH) is a rare condition that especially affects children and displays a wide variety of clinical manifestations. The most common features are bone lesions. There is limited knowledge about extra-osseous affectations of LCH. Examples of targeted systems include skin (55%) and the CNS (35%).

Approximately 25–35% of children with LCH, especially those who show multisystem manifestations, have CNS involvement. Two patterns have been described: granuloma formation and degenerative changes.

Granulomas can develop anywhere in the CNS, the most frequent location being the hypothalamic–hypophyseal axis. MRI shows a loss of normal T1 signal from the neurohypophysis due to a decrease in storage of vasopressin, which leads to diabetes insipidus, a distinctive characteristic of the condition. MRI also displays an abnormal thickening and increased contrast enhancement of the hypophysis due to histiocytic infiltration.

Degenerative changes tend to occur in the cerebellum, especially in the dentate nuclei in a bilateral, symmetrical manner. Less often, the basal ganglia and brainstem are affected. These lesions cause inflammatory diffuse axonal damage, which leads to demyelination and, ultimately, atrophy. MRI shows hypointense lesions in T1-weighted MR images and iso or hyperintense lesions in T2-weighted MR images, which enhance with contrast proportionally to their degree of activity.

Lateral radiographs of the skull show multiple geographic lytic lesions of the bone with well-defined, non-sclerosed margins (Fig. 2.17). The MR T1-weighted image shows loss of the normal high signal from the neurohypophysis (Fig. 2.18). Bilateral, symmetric lesions of the white matter that are hypointense in T1-weighted images (not shown) and hyperintense in T2-weighted images characterize the cerebellar involvement (Fig. 2.19). After administering contrast, the hypophysis shows a normal uptake (not seen here) and the lytic lesions show a significant enhancement (Fig. 2.20). On the other hand, the cerebellar lesions do not present contrast uptake, which signifies demyelination and gliosis.

Figure 2.17

Figure 2.18

Figure 2.19

Figure 2.20

## Comments

## Imaging Findings

## Case 2.6

### Hemangioma of Infancy

Cristina Bravo Bravo and Pascual García-Herrera Taillefer

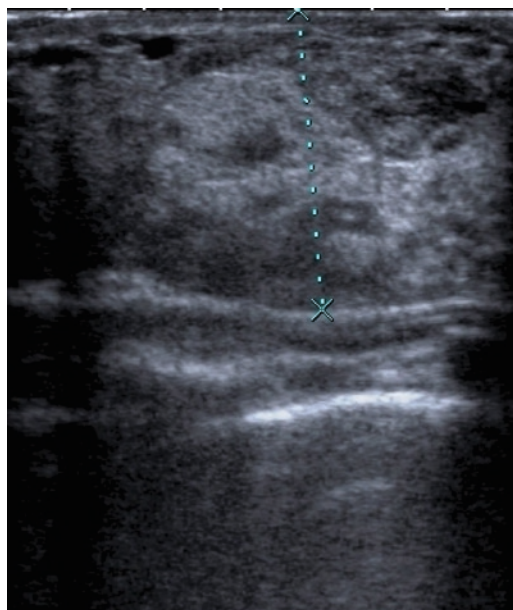


Fig. 2.21

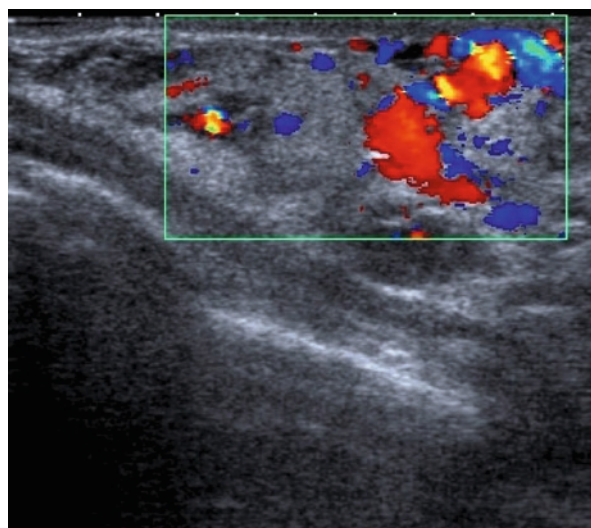


Fig. 2.22

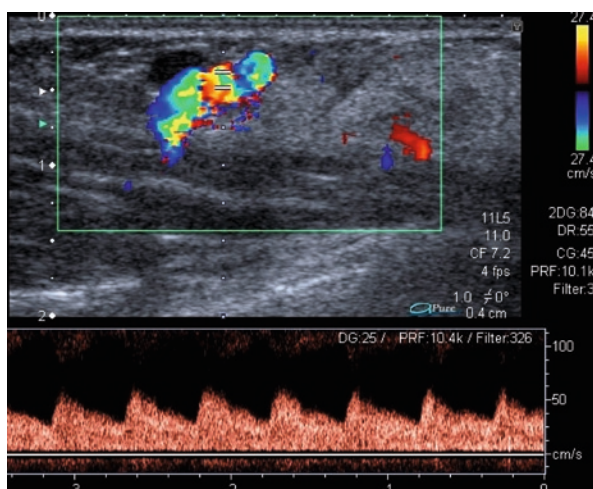


Fig. 2.23

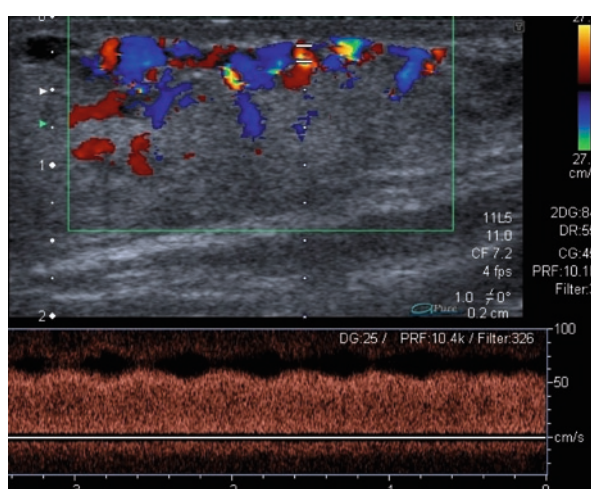


Fig. 2.24

A 2-month-old girl presents with a rapidly growing bluish tumor on the right mammary gland that had appeared at approximately 2–3 weeks of age.

Hemangiomas are the most common soft-tissue tumors of infancy. They are usually absent at birth and appear between the second and sixth week of life. Hemangiomas show a characteristic clinical evolution: a phase of rapid proliferation (3–9 months) followed by a period of relative stability and finally, a phase of slow involution (18 months up to 10 years of age). Most are diagnosed clinically and do not require further diagnostic studies or treatment. The GLU-T1 immunohistochemical marker serves to differentiate the hemangioma of infancy from congenital hemangiomas and vascular malformations. Ultrasound and MRI are indicated in atypical cases and in lesions that are large in size in order to evaluate the extent of compromise and its relation with neighboring structures. Furthermore, imaging may aid in assessing associated abnormalities such as lumbar hemangiomas, spinal dysraphisms, segmented facial hemangiomas, PHACE syndrome, multiple cutaneous hemangiomas, and diffuse neonatal hemangiomatosis.

Sonographically, these tumors are well-delineated, lobulated, and show variable echogenicity. On gray scale, US vascular structures are not usually identified; although, on occasion, peripheral supplying arteries can be seen. Doppler US reveals high vessel density with high systolic arterial velocities and a low resistance pattern. There is little or no evidence of arteriovenous shunting, and veins show a monophasic pattern. Diagnostic criteria for hemangiomas of infancy include the presence of five or more blood vessels by square centimeters of area and displacement of the systolic frequency by 2 kHz or more. During the involutive phase, the size of the lesion and the number of vessels decrease, but arterial velocities remain unchanged.

Possible differential diagnoses include vascular malformations and other soft-tissue tumors. If a lesion does not meet the diagnostic criteria for hemangioma, a biopsy must be taken.

Ultrasound shows a predominantly echogenic mass with heterogeneous echo-structure and peripheral blood vessels (Fig. 2.21). Color Doppler shows a high vessel density with occasional areas of turbulent blood flow (Fig. 2.22). Spectral Doppler (Fig. 2.23) displays a low-resistance vascular pattern with high systolic velocities and a pulsatile venous flow due to small arteriovenous fistulas (Fig. 2.24). These findings are consistent with a hemangioma of infancy in a proliferative phase.

Figure 2.21

Figure 2.22

Figure 2.23

Figure 2.24

## Comments

## Imaging Findings



## Case 2.7

## Vascular Lesion of the Face

Sara M. Koenig and Juan E. Gutiérrez

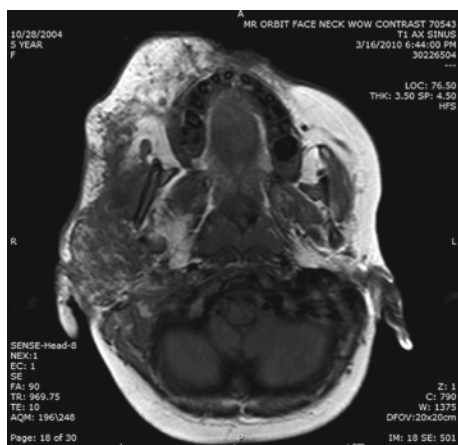


Fig. 2.25

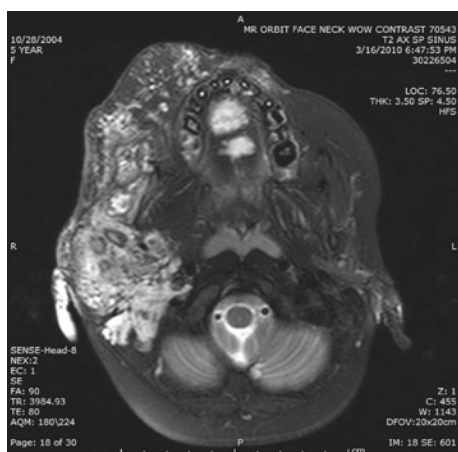


Fig. 2.27

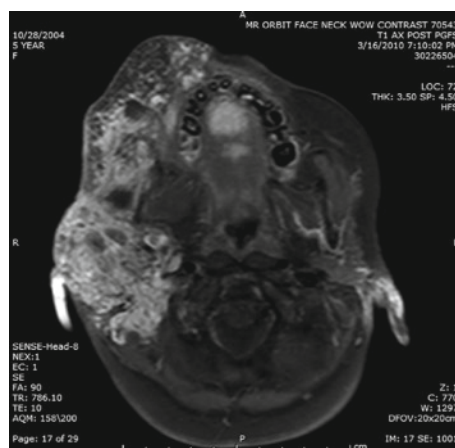


Fig. 2.26

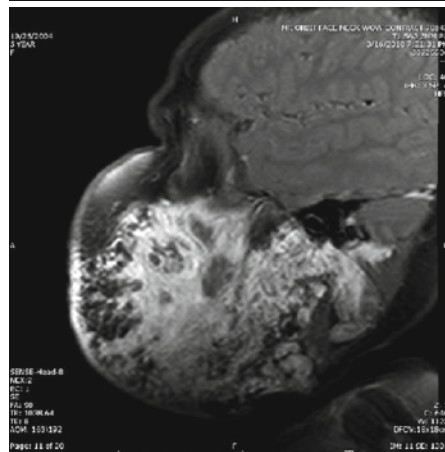


Fig. 2.28

A 5-year-old female presents with a left-sided facial vascular malformation and history of prior surgical interventions.

Capillary hemangiomas and venous malformations are each typically benign lesions of vascular channels. Hemangiomas are benign endothelial cell neoplasms that commonly occur in children, especially under the age of 12 months. A red-colored lesion with a lobulated appearance appears on the skin, from which rapid growth may occur within the first 12 months of life. Angiography reveals a capillary lesion with well-demarcated dense opacification throughout, and with substantial blood flow arising from dilated arteries and dilated venous drainage. These benign lesions are typically harmless and only pose a cosmetic defect that typically stabilizes within a year of age and, in some cases, regress within a few years. In some circumstances, hemangiomas may cause functional impairment that requires aggressive treatment. Functional impairments may include impairment of vision development, feeding patterns, or language due to location on the eyelid, lips, or inside the mouth. Other defects may include hemorrhage or airway defects due to obstruction. Treatment typically consists of surgical resection, laser coagulation, or embolization, whereas endovascular interventions are only used in extreme cases that involve thrombocytopenia and bleeding diathesis.

Arteriovenous malformations vary from hemangiomas in that they are a benign growth of vascular channels with little and poorly demarcated opacification during angiography. Direct percutaneous injection of contrast typically optimizes opacification for imaging. Arteriovenous and venous malformations are typically treated conservatively, although complications such as hemorrhage, infiltration, or osseous involvement may require surgical resection or endovascular treatments.

Axial unenhanced T1-w (Fig. 2.25), enhanced T1-w (Fig. 2.26), axial T2-w (Fig. 2.27) and coronal and sagittal T2-w (Fig. 2.28) MR images exhibit the large, complex lesion with cystic components and avid enhancement involving the right side of the face (and posterolateral aspect of the neck ending at the right posterior triangle of the neck). This mass involves the oral cavity, masticator compartment, parotid space, and submental regions. The imaging characteristics of this lesion are compatible with a large venous malformation.

Figure 2.25

Figure 2.26

Figure 2.27

Figure 2.28

## Comments

## Imaging Findings

**Case 2.8****Retinoblastoma**

Juan E. Gutiérrez and Sara M. Koenig

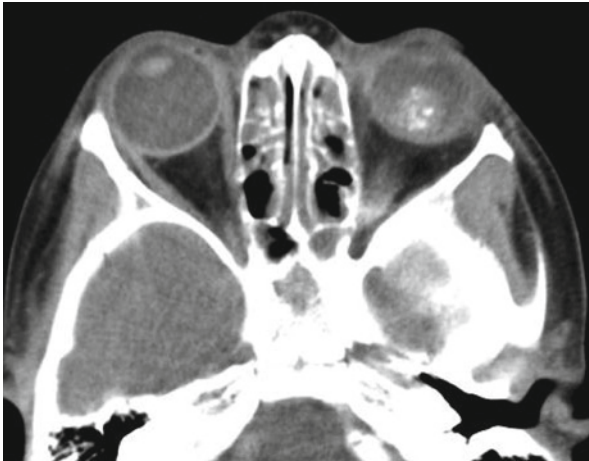


Fig. 2.29



Fig. 2.30

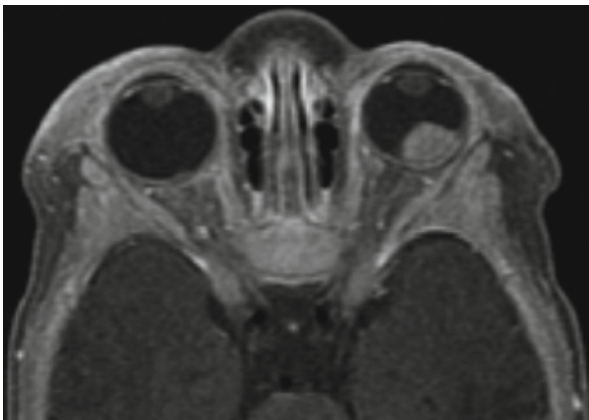


Fig. 2.31

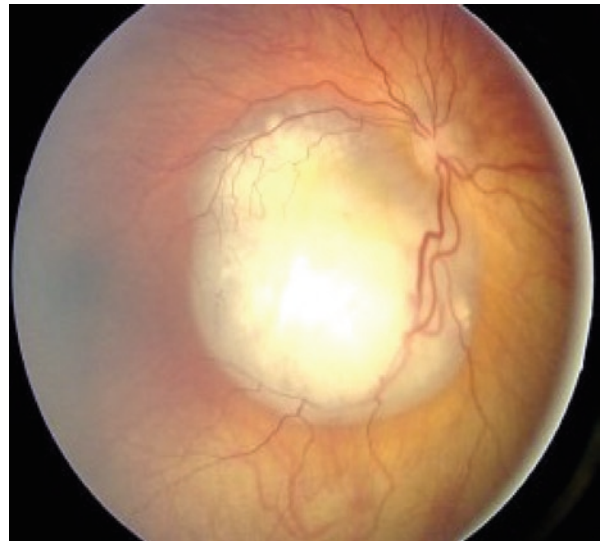


Fig. 2.32

A 14-month old male presents with an abnormal fundoscopic exam. His mother has a history of bilateral retinoblastoma. Calcifications appear in the soft tissue of the left eye.

Retinoblastoma (RB) is the most common intraocular malignancy in children. Of all retinoblastoma cases 70–80% are in infants less than 2 years old, and these tumors arise from retinal tissue. The most common presentation of retinoblastoma is leukocoria in early childhood, or a whitening of the retina seen on fundoscopic exam.

The most common mutation associated with RB is in the RB1 tumor suppressor gene on chromosome 13 controlling progression of the cell cycle, and greater than 200 mutations have been found. Most cases are sporadic; however, 10% are heritable as an autosomal dominant disease. Hereditary RB is often bilateral (rather than unilateral), and among all cases of retinoblastoma approximately 30% are bilateral and 30% multifocal. “Trilateral RB” occurs in approximately 4–7% of individuals with bilateral retinoblastoma, where a small cell intracranial tumor concurrently develops. These individuals often present at an earlier age than those with unilateral or sporadic retinoblastoma, have a higher likelihood of hereditary retinoblastoma, may develop additional tumors in the pineal, suprasellar, or fourth ventricular regions, and have a poor prognosis.

Imaging studies triangle usually starts with US. On CT scan revealing a high-density mass with calcifications arising from the retina, although margins may vary from well delineated to very unclear. Calcification within these tumors is considered a primary factor in the radiological diagnosis of RB. Retinal detachment is often seen due to the local mass effect of the tumor, and extension of the tumor often follows the optic nerve or the lymphatics of the orbit. MRI should be used in patients with suspected intracranial spread of the tumor or with bilateral retinoblastoma, and increased attention should be given to areas mentioned above: the pineal, suprasellar, and fourth ventricular regions. MR images are more sensitive to the spread of the tumor along the optic nerve and, with contrast, illustrate a well-enhanced intraocular mass. Unenhanced T1- and T2-weighted MRI show a mass at approximately the same intensity as normal gray matter.

CT without and with contrast, show of the left orbit revealing retinal high density enhancing mass with calcifications (Figs. 2.29 and 2.30). MRI axial Fat-Sat post-contrast image reveals left retinal detachment due to a solid mass with homogenous enhancement (Fig. 2.31). Fundoscopic appearance of the lesion (Fig. 2.32).

Figure 2.29

Figure 2.30

Figure 2.31

Figure 2.32

## Comments

## Image Findings

## Case 2.9

### Tuberous Sclerosis

Ana Alonso Murciano and María I. Martínez León

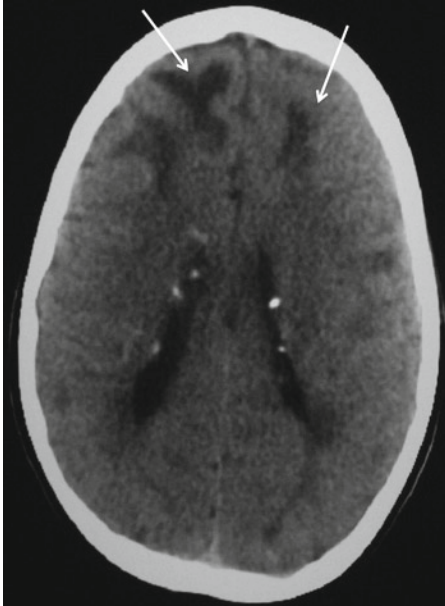


Fig. 2.33

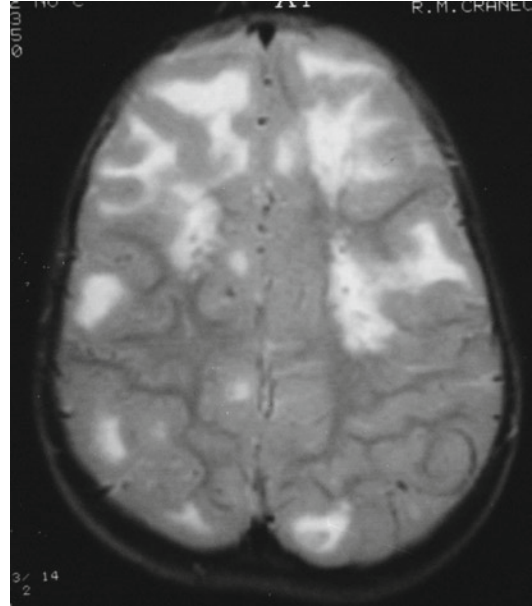


Fig. 2.34

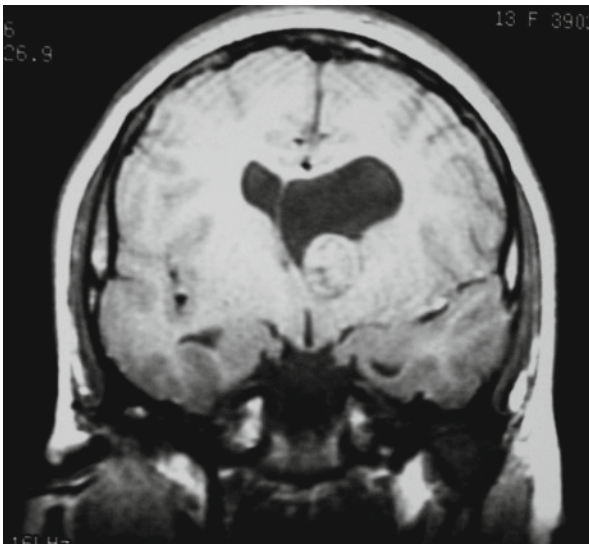


Fig. 2.35



Fig. 2.36



Young boy presents with known congenital syndrome and uncontrolled seizures.

Tuberous Sclerosis (TS) is an autosomal dominant neurocutaneous syndrome characterized by the presence of benign congenital tumors in multiple organs. The diagnosis is usually established on the basis of major and minor diagnostic criteria applied to physical or radiological findings. The classical triad of epilepsy, mental retardation, and sebaceous adenoma is rare. TS is caused by a mutation of two tumor-suppressing genes known as TSC1 and TSC2. Mutation in TSC2 tends to result in a more severe form of the disease and a higher number of cortical tubers (CTs). Neurological involvement is seen in 95–100% of cases and includes CTs, subependymal nodules (SNs), subependymal giant-cell astrocytomas (SGCAs), and white matter abnormalities. Other common manifestations are renal angiomyolipomas (AMLs) (55–75% of cases) and cardiac rhabdomyomas (50–65% of cases).

1. CTs are characterized by the presence of dysmorphic neurons and large astrocytes. Patients with more than six CTs present with a greater difficulty to control seizures.
2. SNs and SGCAs represent hamartomatous changes in subependymal tissue. SNs are frequently calcified. SGCAs are typically located in the foramen of Monro and have a benign course. Nevertheless, due to their location, they may cause obstructive hydrocephalus.
3. White matter alterations include superficial white matter abnormalities associated with cortical tubers, radial white matter bands, and cyst-like lesions.
4. Cardiac rhabdomyomas are benign striated muscle tumors that are commonly located in the ventricular septum and may be single or multiple. Most of them do not cause clinical manifestations and spontaneous regression may occur.
5. AMLs are characterized by variable amounts of abnormal vessels and immature smooth-muscle and fat cells. In patients with TS, AMLs usually develops at a younger age and tends to be larger in size, bilateral, and multiple.

CT without contrast shows calcified subependymal nodules and frontal bilateral cortical tubers (arrows) (Fig. 2.33). Axial T2-weighted MR image depicts multiple cortical tubers and white matter abnormalities (Fig. 2.34). Coronal FLAIR MR image displays a left subependymal giant cell astrocytoma (Fig. 2.35). CT with contrast shows bilateral renal angiomyolipomas (Fig. 2.36).

Figure 2.33

Figure 2.34

Figure 2.35

Figure 2.36

## Comments

## Imaging Findings

## Case 2.10

### Neurofibromatosis Type 1

Inés Solís Muñiz

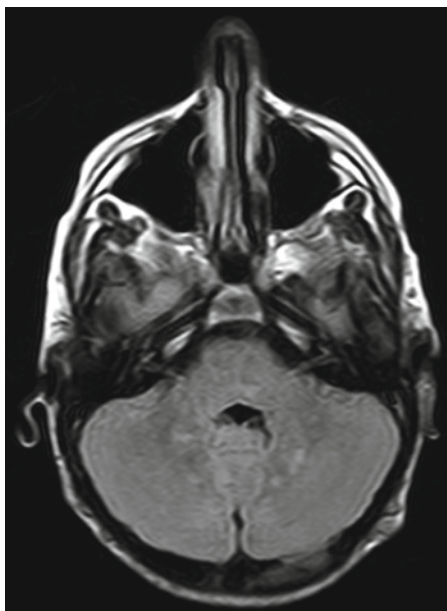


Fig. 2.37

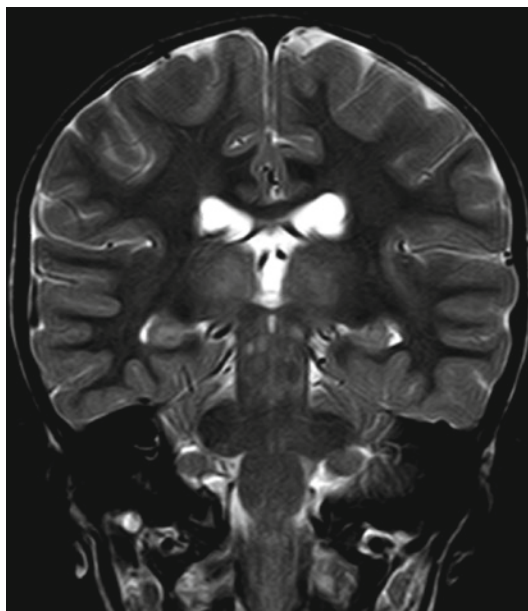


Fig. 2.38

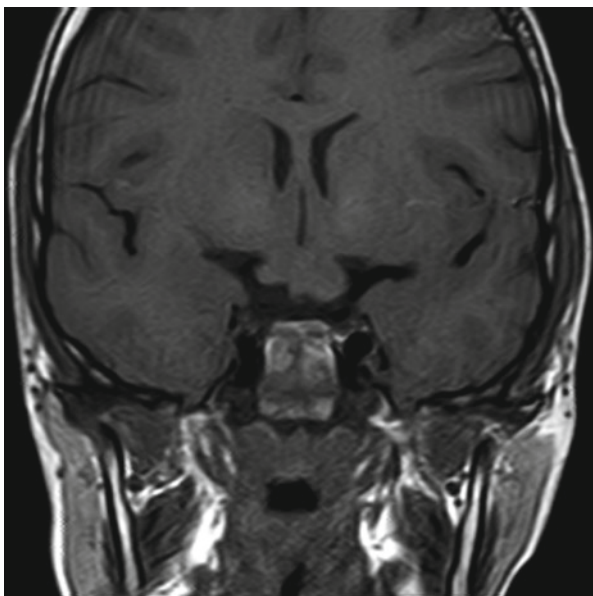


Fig. 2.39

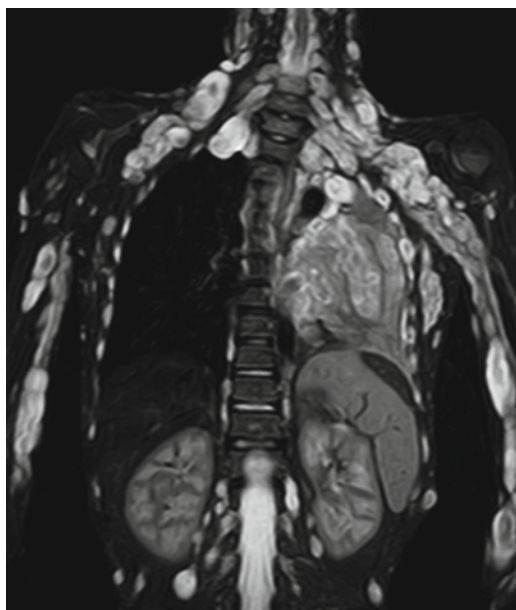


Fig. 2.40

A 12-year-old boy with known neurofibromatosis type 1 presents with multiple *café-au-lait* spots, visual disturbances, mild mental retardation, and scoliosis.

Neurofibromatosis type I (NF-1), formerly known as von Recklinghausen disease, is a relatively common (1/3,000 live births) autosomal dominant genetic disorder classified as a neurocutaneous syndrome or phakomatosis. Diagnosis is usually established in childhood based on a series of well-known major and minor criteria.

Apart from the dermatological manifestations of the condition (*café-au-lait* spots, axillary freckles, Lisch nodules of the iris), neurological abnormalities such as myelin vacuolization (40–90%), and optic tract (30%) and cerebral (1–3%) gliomas can also be identified. Dermal neurofibromas are seen in 90% of cases and plexiform neurofibromas in approximately 30% of patients. While neurofibromas are usually considered benign nerve-sheath tumors, the plexiform variation has shown malignant transformation in up to 10% of cases. Other abnormalities include bone dysplasia (5%) and scoliosis. Patients with NF-1 also have a higher risk of developing genetically related tumors such as rhabdomyosarcomas and neuroblastomas. Close monitoring is required due to their increased tendency to develop both benign and malignant neoplasms.

Imaging studies, specifically MRI, play an important role in the detection, extension assessment, and follow-up of the aforementioned neurological and non-neurological manifestations of the disease.

Surgical resection of symptomatic tumors is currently the first line of treatment.

Axial FLAIR (Fig. 2.37) and coronal T2-weighted (Fig. 2.38) MR images show multiple focal hyperintense lesions of the cerebellar white matter, brainstem, and bilateral thalami. No mass effect or contrast enhancement is observed. These findings are consistent with myelin vacuolization. Coronal T1-weighted MR image shows a predominantly left-sided volume increase of the optic chiasm consistent with glioma (Fig. 2.39). Coronal STIR MR image of the thorax and superior abdomen exhibits a large number of paravertebral, intercostal, and bilateral subcutaneous tumors. Additionally, a large mass can be seen on the left hemithorax with hyperintense lobulations and a central, target-like loss of signal, typical of neurofibromas (Fig. 2.40).

Figure 2.37

Figure 2.38

Figure 2.39

Figure 2.40

## Comments

## Imaging Findings

## Further Reading

### Books

- Barnes L, Eveson JW, Reichart P, Sidransky D (2005) World Health Organization Classification of Tumors: Pathology and genetics of head and neck tumors. Lyon, IARC. p 53
- Barkovich AJ (2000) Pediatric neuroimaging, 3rd edn. Lippincott Williams & Wilkins, Philadelphia, pp 494–496
- Barkovich AJ (2005) Intracranial, orbital, and neck masses of childhood. In: Pediatric neuroimaging, 4th ed. Lippincott Williams & Wilkins, Philadelphia, pp 506–658
- Barkovich AJ (2005b) Pediatric Neuroimaging. Lippincott Williams & Wilkins, Philadelphia
- Barkovich AJ (2005c) Pediatric neuroimaging, 4th edn. Lippincott Williams & Wilkins, Philadelphia, pp 440–459
- Groosman and Yousem. Neuroradiologia. Ed. Marban 2007
- Gutiérrez JE, Restrepo R, Soto JA (eds) (2004) Radiology and diagnostic imaging, 2nd ed, CIB Collection
- Louis DN, Oggki H, Wiestler OD, et al (eds) (2007) World Health Organization Classification of tumours. Pathology and genetics of tumours of the nervous system. IARC, Lyon
- Scott A (2004) Magnetic resonance imaging of the brain and spine, 3rd edn. Lippincott Williams & Wilkins, Philadelphia, pp 1340–1342
- Siegel MJ (2004) Masas de partes blandas. In: Siegel MJ (ed) Ecografía Pediátrica, 2nd ed. pp 651–652

### Web Links

- <http://www.childrenshospital.org/az/Site979/mainpageS979P0.html>
- <http://www.searchmedica.com/search.html?q=pleomorphic%20xanthoastrocytoma>
- [www.radiographics.org](http://www.radiographics.org)
- <http://journals.lww.com/ajsp/pages/default.aspx>
- <http://scielo.isciii.es/scielo.php>
- [www.issva.org](http://www.issva.org) (International Society for the Study of Vascular Anomalies)
- <http://www.mayoclinic.org/intracranial-venous-malformations/>
- <http://www.cancer.gov/cancertopics/types/retinoblastoma>. Retinoblastoma. United States National Cancer Institute
- [www.tuberous-sclerosis.org](http://www.tuberous-sclerosis.org)
- <http://emedicine.medscape.com/article/950151-overview>

### Articles

- Alexiou GA, Stefanaki K, Sfakianos G, Prodromou N (2008) Desmoplastic infantile ganglioglioma: a report of 2 cases and a review of the literature. *Pediatr Neurosurg* 44(5):422–425
- Alkan A, Sigirci A, Kutlu R et al (2005) Neurofibromatosis type 1: diffusion weighted imaging findings of brain. *Eur J Radiol* 56:229–234
- Aoki S, Barkovich JA, Nishimura K et al (1989) Neurofibromatosis types 1 and 2: Cranial MR findings. *Radiology* 172:527–534

- Bächli H, Avoledo P, Gratzl O, Tolnay M (2003) Therapeutic strategies and management of desmoplastic infantile ganglioglioma: two case reports and literature overview. *Childs Nerv Syst* 19(5-6):359–366
- Bagley LJ, Hurst RW, Zimmerman RA, Shields JA, Shields CL, Potter P (2002) Imaging in the trilateral retinoblastoma syndrome. *Pediatr Neurol* 38(2):166–170
- Baisden BL, Brat DJ, Mekhem ER, Rosenblum MK, King AP, Burger PC (2001) Dysembryoplastic neuroepithelial tumor-like neoplasm of the septum pellucidum: a lesion often misdiagnosed as glioma. Report of ten cases. *Am J Surg Pathol* 25:494–499
- Balaji R, Ramachandran K (2009) Imaging of desmoplastic infantile ganglioglioma: a spectroscopic viewpoint. *Childs Nerv Syst* 25(4):497–501
- Baron Y, Barkovich AJ (1999) MR imaging of tuberous sclerosis in neonates and young infants. *AJNR* 20:907–916
- Bilginer B, Sylemezoglu F, Cila A, Akalan N (2009) Intraventricular dysembryoplastic neuroepithelial tumor-like neoplasm with disseminated spinal tumor. *Turk Neurosurg* 19:69–72
- Biswas J, Mani B, Mahesh PS, Patwardhan D, Kumar KS, Badrinath SS (2000) Retinoblastoma in adults: report of three cases and review of the literature. *Surv Ophthalmol* 44(5):409–414
- Boukobza M, Enjolras O et al (1996) Cerebral developmental anomalies associated with head and neck venous malformations. *Am J Neuroradiol* 17:987–994
- Brisse HJ et al (2001) Sonographic, CT, and MR imaging findings in diffuse infiltrative retinoblastoma: report of two cases with histologic comparison. *Am J Neuroradiol* 22:449–504
- Brisse HJ et al (2007) Relevance of CT and MRI in retinoblastoma for the diagnosis of poastlaminar invasion with normal size optic nerve: a retrospective study of 150 patients with histological comparison. *Pediatr Radiol* 37:649–656
- Brouwer PA et al (2009) Dynamic 320-section ct angiography in cranial arteriovenous shunting lesions. *Am J Neuroradiol* 31:767–770
- Catalpete O, Marshall P, Smith TW (2009) Dysembryoplastic neuroepithelial tumor located in pericallosal and intraventricular area in a child. *J Neurosurg Pediatr* 3:456–460
- Cervera-Pierot P, Varlet P, Chodkiewicz JP (1997) Daumas-Duport C. Dysembryoplastic neuroepithelial tumors located in the caudate nucleus area: report of four cases. *Neurosurgery* 40:1065–1070
- Crespo-Rodríguez AM, Smirniotopoulos JG, Rushing EJ (2007) MR and CT imaging of 24 pleomorphic xanthoastrocytomas (PXA) and a review of the literature. *Neuroradiology* 49:307–315
- Crino PB, Nathanson KL, Henske EP (2006) The tuberous sclerosis complex. *N Engl J Med* 355:1345–1356
- Dariusch H et al (2008) Cerebral arteriovenous malformation: Spetzler–Martin classification at subsecond temporal-resolution four-dimensional MR angiography compared with that of DSA. *Radiology* 246:205–213
- DiMario FJ Jr (2004) Brain abnormalities in tuberous sclerosis complex. *J Child Neurol* 1989:650–657
- DiPaolo DP, Zimmerman RA, Rorke LB, Zackai EH, Bilaniuk LT, Yachnis AT (1995) Neurofibromatosis type 1: pathological substrate of high-signal intensity foci in the brain. *Radiology* 195:721–724

- Donnelly LF, Adams DM, Bisset GS (2000) Vascular malformation and hemangiomas: a practical approach in a multidisciplinary clinic. *AJR* 174:597–608
- Drolet BA, Esterly NB, Frieden IJ (1999) Hemangiomas in children. *N Engl J Med* 341:1173–1181
- Dubois J, Garel L (1999) Imaging and therapeutic approach of hemangiomas and vascular malformations in the pediatric age group. *Pediatr Radiol* 29:879–893
- Dubois J et al (1998) Soft-tissue hemangiomas in infants and children: diagnosis using Doppler sonography. *AJR* 171:247–252
- Dubois J, Garel L, David M, Powell J (2002) Vascular soft-tissue tumors in infancy: distinguishing features on Doppler sonography. *AJR* 178:1541–1545
- Dunnick NR (2000) The radiological Society of North America 85th scientific assembly and annual meeting: image interpretation session: 1999. *Radiographics* 20:257–278
- Evans JC, Curtis J (2000) The radiological appearances of tuberous sclerosis. *Br J Radiol* 73:91–98
- Finelli DA, Shurin SB, Bardenstein DS (1995) Trilateral retinoblastoma: two variations. *Am J Neuroradiol* 16:166–170
- Finistis S et al (2009) Nasal Chondromesenchymal hamartoma in a child. *Cardiovasc Intervent Radiol* 32:593–597
- Fishman SJ, Mulliken JB (1993) Hemangiomas and vascular malformations of infancy and childhood. *Pediatr Clin N Am* 40(6):1177–1200
- Fordham LA, Chung CJ, Donnelly LF (2000) Imaging of congenital vascular and lymphatic anomalies of the head and neck. *Neuroimaging Clin N Am* 10:117–136
- Fortman BJ, Kuszyk BS, Urban BA (2001) Neurofibromatosis type 1: a diagnostic mimicker at CT. *Radiographics* 21:601–612
- Fujisawa H, Marukawa K, Hasegawa M, Tohma Y, Hayashi Y, Uchiyama N (2002) Genetic differences between neurocytoma and dysembryoplastic neuroepithelial tumor and oligodendroglial tumors. *J Neurosurg* 97:1350–1355
- Galluzzi P, Hadjistilianou T et al (2009) Is CT still useful in the study protocol of retinoblastoma? *Am J Neuroradiol* 30:1760–1765
- Ganesan K, Desai Sm, Udawadia-Hegde A (2006) Non-infantile variant of desmoplastic ganglioglioma: a report of 2 cases. *Pediatr Radiol* 36(6):541–545
- Geibprasert S et al (2010) Radiologic assessment of brain arteriovenous malformations: what clinicians need to know. *Radiographics* 30:483–501
- Gorincour G, Kokta V, Rypens F, Garel J, Powell J, Dubois J (2005) Imaging characteristics of two subtypes of congenital hemangiomas: rapidly involuting congenital hemangiomas and non-involuting congenital hemangiomas. *Pediatr Radiol* 35:1178–1185
- Goyal CM, Armstrong D (2002) Venous vascular malformations in pediatric patients: comparison of results of alcohol sclerotherapy with proposed MR imaging classification. *Radiology* 223:639–644
- Grois N, Prayer D, Prosch H, Minkov M, Potschger U, Gadner H (2004) Course and clinical impact of magnetic resonance imaging findings in diabetes insipidus associated with Langerhans cell histiocytosis. *Pediatr Blood Cancer* 43:59–65
- Grois N, Prayer D, Prosch H, Lassmann H (2005) Neuropathology of CNS disease in Langerhans cell histiocytosis. *CNS LCH Co-operative Group. Brain* 128:829–838
- Guesmi H, Houtteville JP, Courthéoux P, Derlon JM, Chapon F (1999) Dysembryoplastic neuroepithelial tumors. Report of 8 cases including two with unusual localization. *Neurochirurgie* 45:190–200
- Harter DH, Omeis I, Forman S, Braun A (2006) Endoscopic resection of an intraventricular dysembryoplastic neuroepithelial tumor of the septum pellucidum. *Pediatr Neurosurg* 42:105–107
- Hoving EW, Kros JM, Groninger E, den Dunnen WF (2008) Desmoplastic infantile ganglioglioma with a malignant course. *J Neurosurg Pediatr* 1(1):95–98
- Hoyosa M, Naito H, Nihei K (1999) Neurological prognosis correlated with variations over time in the number of subependymal nodules in tuberous sclerosis. *Brain Dev* 21:544–547
- Hsueh C, Hsueh S, Crussi FG et al (2001) Nasal chondromesenchymal hamartoma in children. *Arch Pathol Lab Med* 125(3):400–403
- Ishizawa K, Terao S, Kobayashi K, Yoshida K, Hirose T (2007) A neuroepithelial tumor showing combined histological features of dysembryoplastic neuroepithelial tumor and pleomorphic xanthoastrocytoma – a case report and review of the literature. *Clin Neuropathol* 26:169–175
- James SH, Halliday WC, Branson HM (2010) Trilateral retinoblastoma. *Radiographics* 30:833–837
- Johnson C et al (2006) Nasal chondromesenchymal hamartoma: radiographic and histopathologic analysis of a rare pediatric tumor. *Pediatr Radiol* 37:101–104
- Kang Jun, Young Ok Hong, Gung Hwan Ahn, Young Min Kim, Hee Jeong Cha, Hye-Jeong Choi (2007) Nasal chondromesenchymal hamartoma: a case report. *Korean J Pathol* 41:258–62
- Kato K, Reiko I, Yukichi T, Masamichi H, Kennichi S (Jan 2002) Nasal chondromesenchymal hamartoma of infancy: the first Japanese case report. *Pathol Int* 49(8):731–736
- Kepes JJ, Rubinstein LJ, Eng LF (1979) Pleomorphic xanthoastrocytoma: a distinctive meningocerebral glioma of young subjects with relatively favorable prognosis. A study of 12 cases. *Cancer* 44:1839–1852
- Kim EY, Choi JU, Kim TS, Kim DI, Kim KY (1995) Huge Langerhans cell histiocytosis granuloma of choroids plexus in a child with Hand-Schüller-Christian disease. *J Neurosurg* 83:1080–1084
- Kim B, Park SH, Min HS, Rhee JS, Wang KC (2004) Nasal chondromesenchymal hamartoma of infancy clinically mimicking meningoencephalocele. *Pediatr Neurosurg* 40(3):136–140
- Kim JE et al (2009) Nasal chondromesenchymal hamartoma: CT and MR imaging findings. *Korean J Radiol* 10(4):216–419
- Koeller KK, Henry JM (2001) From the archives of the AFIP: superficial gliomas: radiologic-pathologic correlation. *Radiographics* 21:1533–1556
- Lee BB, Bergan JJ (2002) Advanced management of congenital vascular malformations: a multidisciplinary approach. *Cardiovasc Surg* 10(6):523–533
- Legiehn GM, Heran MK (2009) Venous malformations: classification, development, diagnosis, and interventional radiologic management. *Radiol Clin N Am* 46:545–597
- Ak L, Robson WL (2007) Tuberous sclerosis complex: a review. *J Pediatr Health Care* 21:108–114



- Lellouch-Tubiana KS, Kulkarni AV A, Sainte-Rose C (2006) Pleomorphic xanthoastrocytoma of the cerebellopontine angle in a child. *Childs Nerv Syst* 22:1479–1482
- Levy AD, Patel N, Dow N, Abbott RM, Miettinen M, Sobin LH (2005) From the Archives of the AFIP. Abdominal neoplasms in patients with neurofibromatosis type 1: radiologic-pathologic correlation. *RadioGraphics* 25:455–480
- Lopes Ferraz Filho JR, Munis MP, Soares Souza A, Sanches RA, Goloni-Bertollo EM, Pavarino-Bertelli EC (2008) Unidentified bright objects on brain MRI in children as a diagnostic criterion for neurofibromatosis type 1. *Pediatr Radiol* 38:305–310
- Maghnie M, Aricò M, Villa A, Genovese E, Beluffi G, Severi F (1992) MR of the hypothalamic-pituitary axis in Langerhans cell histiocytosis. *AJNR* 13:1365–1371
- Maher CO, White JB, Scheithauer BW, Raffel C (2008) Recurrence of dysembryoplastic neuroepithelial tumor following resection. *Pediatr Neurosurg* 44:333–336
- Marton E, Feletti A, Orvieto E, Longatti P (2007) Malignant progression in pleomorphic xanthoastrocytoma: personal experience and review of the literature. *J Neurol Sci* 252:144–153
- Mautner VF, Hartmann M, Kluwe L, Friedrich RE, Fünsterer C (2006) MRI growth pattern of plexiform neurofibromas in patients with neurofibromatosis type 1. *Neuroradiology* 48:160–165
- McDermott MB, Bonder BT, Dehner LP (1998) Nasal chondromesenchymal hamartoma: an upper respiratory tract analogue of the chest wall mesenchymal hamartoma. *Am J Surg Pathol* 22(4):425–433
- Menor F, Martí-Bonmati L, Mulas F, Poyatos C, Cortina H (1992) Neuroimaging in tuberous sclerosis: a clinicoradiological evaluation in pediatric patients. *Pediatric Radiol* 22(7):485–489
- Menor F, Martí-Bonmati L, Arana E, Poyatos C, Cortina H (1998) Neurofibromatosis type 1 in children: MR imaging and follow-up studies of central nervous system findings. *Eur J Radiol* 26:121–131
- Metry DW, Hebert AA (2000) Benign cutaneous vascular tumors of infancy. when to worry, what to do. *Arch Dermatol* 136:905–914
- Moon HH et al (1999) Craniofacial arteriovenous malformation: preoperative embolization with direct puncture and injection of n-butyl cyanoacrylate. *Radiology* 211:661–666
- Mulliken JB, Glowacki J (1982) Hemangiomas and vascular malformations in infants and children: a classification based on endothelial characteristics. *Plas Reconstr Surg* 69:412–420
- Murdo Sk Mc Jr, Moore SG, Brant-Zawadzki M, Berg BO, Koch T, Newton TH et al (1987) Mr imaging of intracranial tuberous sclerosis. *AJR* 148:791–796
- Nakagawa T, Sakamoto T, Ito J (2009) Nasal chondromesenchymal hamartoma in an adolescent. *Int J Pediatr Otorhinolaryngol* 4:111–113
- Narayanan V (2003) Tuberous sclerosis complex: genetics to pathogenesis. *Pediatr Neurol* 29:404–409
- Norman ES, Bergman S, Trupiano JK (2004) Nasal chondromesenchymal hamartoma: report of a case and review of the literature. *Pediatr Dev Pathol* 7(5):517–520
- Okazaki T, Kageji T, Matsuzaki K, Horiguchi H, Hirose T, Watanabe H et al (2009) Primary anaplastic pleomorphic xanthoastrocytoma with widespread neuroaxis dissemination at diagnosis – a pediatric case report and review of the literature. *J Neurooncol* 94:431–437
- Passone E, Pizzolitto S, D’Agostini S, Skrap M, Gardiman MP, Nocerino A et al (2006) Non-anaplastic pleomorphic xanthoastrocytoma with neuroradiological evidence of leptomeningeal dissemination. *Childs Nerv Syst* 22:614–618
- Patel HJ, Burrows PE, Kozakewich HP, Zurakowski D, Mulliken J (2000) Soft-tissue vascular anomalies: utility of US for diagnosis. *Radiology* 214:747–754
- Petropoulou K, Whiteman ML, Altman NR, Bruce J, Morrison G (1995) CT and MR of pleomorphic xanthoastrocytoma: unusual biologic behavior. *J Comput Assist Tomogr* 19:860–865
- Poe LB, Dubowy RL, Hochhauser L, Collins GH, Crosley CJ, Kanzer MD et al (1994) Demyelinating and gliotic cerebellar lesions in Langerhans cell histiocytosis. *AJNR* 15:1921–1928
- Prayer D, Grois N, Prosch H, Gadner H, Barkovich AJ (2004) MR imaging presentation of intracranial disease associated with Langerhans cell histiocytosis. *AJNR* 25:880–891
- Provenzale JM, Gururangan S, Klintworth G (2004) Trilateral retinoblastoma: clinical and radiologic progression. *AJR* 183:505–511
- Robson CD (2010) Imaging of head and neck neoplasms in children. *Pediatr Radiol* 40:499–509
- Rodjan F, Graaf P et al (2010) Brain abnormalities on MR imaging in patients with retinoblastoma. *Am J Neuroradiol* 31:237–245
- Rosenfield NS, Abrahams J, Komp D (1990) Brain MRI in patients with Langerhans cell histiocytosis: findings and enhancement with Gd-DTPA. *Pediatr Radiol* 20:433–436
- Saito T, Sugiyama K, Yamasaki F, Tominaga A, Kusu K, Takeshima Y (2008) Familial occurrence of dysembryoplastic neuroepithelial tumor-like neoplasm of the septum pellucidum: case report. *Neurosurgery* 63:370–372
- Sevick RJ, Barkovich AJ, Edwards MS et al (1992) Evolution of white matter lesions in neurofibromatosis type 1: MR findings. *AJR* 159:171–175
- Shin JH, Lee HK, Khang SK, Kim DW, Jeong AK, Ahn KJ et al (2002) Neuronal tumors of the central nervous system: radiologic findings and pathologic correlation. *Radiographics* 22:1177–1189
- Smidt S, Eich G, Hanquinet S, Tschäppeler H, Waibel P, Gudinchet F (2004) Extra-osseous involvement of Langerhans’ cell histiocytosis in children. *Pediatr Radiol* 34:313–321
- Smidt S, Eich G, Geoffroy A, Hanquinet S, Waibel P, Wolf R et al (2008) Extraosseous Langerhans cell histiocytosis in children. *Radiographics* 28:707–726
- Spence J, Krings T et al (2010) Percutaneous sclerotherapy for facial venous malformations: subjective clinical and objective MR imaging follow-up results. *Am J Neuroradiology* 31:955–960
- Strothmann JM, Ginsberg LE, Stanton C (1995) Langerhans cell histiocytosis involving the corpus callosum and cerebellum: gadolinium-enhanced MRI. *Neuroradiology* 37:289–292
- Sugita Y, Irie K, Ohshima K, Hitotsumatsu T, Sato O, Arimura K (2009) Pleomorphic xanthoastrocytoma as a component of temporal lobe cystic ganglioglioma: a case report. *Brain Tumor Pathol* 26:31–36
- Takeshima H, Kawahara Y, Hirano H, Obara S, Niino M, Kuratsu J (2003) Postoperative regression of desmoplastic infantile gangliogliomas: report of two cases. *Neurosurgery* 53(4):979–983

- Tamburrini G, Colosimo C Jr, Giangaspero F, Riccardi R, Di Rocco C (2003) Desmoplastic infantile ganglioglioma. *Childs Nerv Syst* 19(5-6):292-297
- Umeoka S, Koyama T, Miki Y, Akai M, Tsutsui K, Togashi K (2004) Pictorial review of tuberous sclerosis in various organs. *Radiographics*; Sept 4, on line
- Yamasaki F, Kurisy K, Satoh K, Arita K, Sugiyama K, Ohtaki M (2005) Apparent diffusion coefficient of human brain tumors at MR imaging. *Radiology* 235:985-991
- Zacharia TT, Jaramillo D, Poussaint TY, Korf B (2005) MR imaging of abdominopelvic involvement in neurofibromatosis type 1: a review of 43 patients. *Pediatr Radiol* 35:317-322
-

Learning Pediatric Imaging

100 Essential Cases

Martínez-León, M.I.; Ceres-Ruiz, L.; Gutierrez, J.E.

2011, XIX, 243 p. 400 illus., 164 illus. in color., Softcover

ISBN: 978-3-642-16891-8